

Hybrid Higher-Order Topological Skin Modes in the Two-Dimensional Su–Schrieffer–Heeger Model with Nonreciprocal Hoppings

Hiomasa Wakao

Graduate School of Pure and Applied Sciences, University of Tsukuba, Tsukuba, Ibaraki 305-8571, Japan

The coexistence of edge states and skin effects provides the topologically protected localized states at the corners of two-dimensional systems. In this paper, we realize such corner states in the two-dimensional Su–Schrieffer–Heeger model with the nonreciprocal hoppings. For the characterization of the real line gap topology, we introduce the \mathbb{Z}_4 Berry phase protected by generalized four-fold rotational symmetry. From the physical picture of the adiabatic connection, we find that the value of the \mathbb{Z}_4 Berry predicts the position of edge states. Additionally, by using the winding number, we characterize the point gap topology of the edge spectra. From the results of these characterizations by the first-order topological invariants, we find that the pair of values of the \mathbb{Z}_4 Berry phase and the winding number yields the position of the topologically protected localized states.

Introduction: Topological materials which are characterized by the topology in the bulk have been actively pursued.^{1–8)} Additionally, the description of these materials are enriched by symmetry.^{9–15)} For instance, the presence of time-reversal symmetry provides the \mathbb{Z}_2 topological properties.⁹⁾ Moreover, it turns out that crystalline symmetry plays a key role for the determination of the band topology.^{16–26)} For example, the coexistence of the time-reversal symmetry and inversion symmetry enables us to introduce the form of \mathbb{Z}_2 indicator determined from the parity at the high-symmetry points in the two-dimensional Brillouin zone.¹⁷⁾

In the past decades, the notion of the topological protection has been extended to a new area: the non-Hermitian systems.^{27–32)} Since the eigenvalues may become complex, many exotic topological phenomena have been provided,^{33–46)} such as the skin effects^{47–56)} and exceptional points (rings).^{57–67)} Particularly, a distinct difference from the case in Hermitian systems is the emergence of two types of the gap, i.e. a line gap and a point gap.⁴⁴⁾ While the line gap topology can be understood by mapping onto the Hermitian cases, the nontrivial point gap topology provides novel phenomena without analogies in the Hermitian case, such as the anomalous sensitivity of the energy spectrum to the presence or absence of boundaries, i.e., the skin effect. In addition, as is the case for the Hermitian systems, these unique topological phenomena are enriched by symmetry.^{68–84)} These phenomena have been reported in a wide range of systems such as open quantum systems,^{58, 85, 86)} electrical circuits,^{74, 87–91)} phononic systems,^{92–94)} and photonic crystals,^{95–98)} and so on.

Along with the above developments, a novel class of topological insulators has been extensively investigated, which is called higher-order topological insulators. In d -dimensional systems, while the conventional topological insulators host $(d - 1)$ -dimensional boundary states, higher-order topological insulators host $(d - 2)$ - or fewer dimensional boundary states.^{99–116)} For the characterization of the topological phase and the prediction of the emergence of these unique boundary states, many efforts have been devoted. Remarkably, the presence of crystalline symmetry plays an important role for the description of the higher-order topology.^{99–103, 107–116)}

Recently, the notion of the higher-order topology has also

been extended to non-Hermitian systems.^{117–120)} In particular, the coexistence of edge states and the skin effect in two-dimensional systems provides the topologically protected corner states, which are called the hybrid higher-order topological skin modes.^{121–127)} These novel states in non-Hermitian systems represent a kind of the higher-order skin effect.^{128–130)} Furthermore, these unique localized states are characterized by the first- and second-order topological invariants such as the Chern number,^{121, 124)} the Wess–Sumino term,¹²⁸⁾ and the symmetry indicator.^{77, 129)}

In this paper, we demonstrate the realization of the hybrid higher-order topological skin modes in the two-dimensional Su–Schrieffer–Heeger (SSH) model with the nonreciprocal hoppings. Specifically, we characterize the first-order topology by using \mathbb{Z}_4 Berry phase protected by generalized four-fold rotational symmetry and the winding number on the cylinder geometry. From the nontrivial value of the \mathbb{Z}_4 Berry phase, we show that there exists the bulk-edge correspondence between this topological invariant and edge states. Additionally, by using the winding number, we realize the skin effect arising from the energy spectra of edge states. Combining the \mathbb{Z}_4 Berry phase and the nontrivial point gap topology of these edge spectra, we demonstrate that the pair of these topological invariants indicates the position of the localized corner in two dimension.

Two-Dimensional Su–Schrieffer–Heeger Model with the Nonreciprocal Hoppings: We consider the two-dimensional SSH model with the nonreciprocal hoppings [see Fig. 1 (a)]. The red and blue lines denote the nonreciprocal hoppings. Specifically, the hoppings along the red and blue arrows are $t_1 + \gamma_1$ and $t_2 + \gamma_2$, respectively. The hoppings opposite to the red and blue arrows are $t_1 - \gamma_1$ and $t_2 - \gamma_2$, respectively.

Firstly, we consider the energy spectrum under the periodic boundary condition. The Hamiltonian is

$$H = \sum_{\vec{k}} \vec{c}^\dagger(\vec{k}) h(\vec{k}) \vec{c}(\vec{k}), \quad (1)$$

with $\vec{c}(\vec{k}) = (c_1(\vec{k}), c_2(\vec{k}), c_3(\vec{k}), c_4(\vec{k}))^T$ being the vector of the annihilate operators. Here, the explicit form of $h(\vec{k})$ is

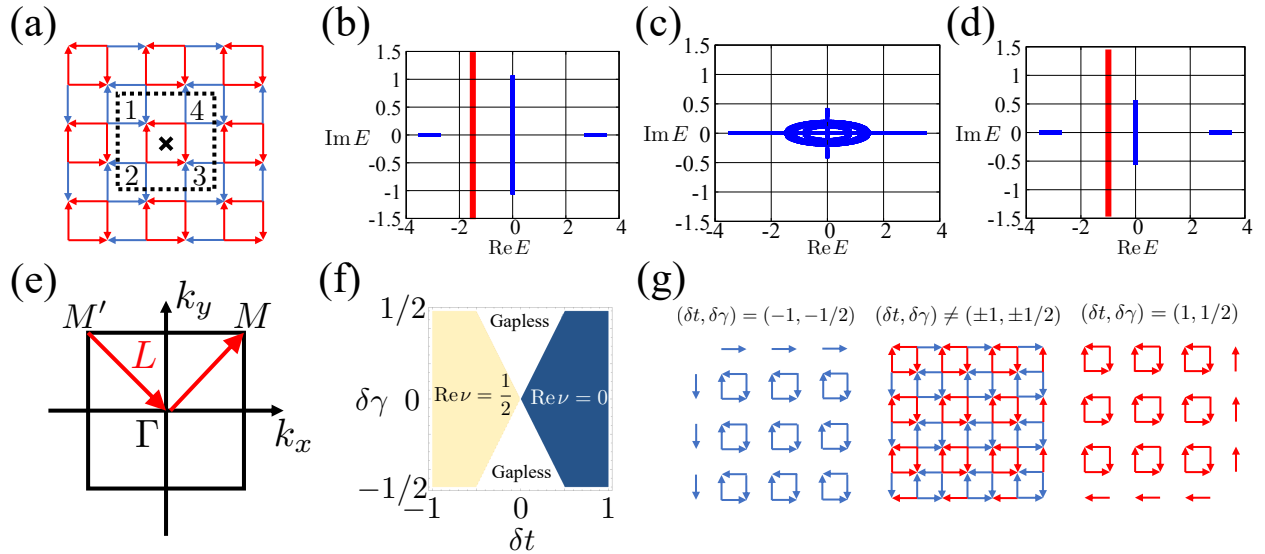


Fig. 1. (Color online) (a) Schematic figure of the two-dimensional SSH model with the nonreciprocal hoppings. The unit cell is enclosed by the black dashed box. The cross denotes the center of the generalized four-fold rotation. (b), (c), and (d) show the energy spectrum for $(\delta t, \delta\gamma) = (-0.7, 0.1)$, $(0, 0.1)$ and $(0.7, 0.1)$. Red lines denote the real line gaps where we focus. (e) Sketch of the Brillouin zone and the path of the integration in Eq. (15). The path L connect high-symmetry points Γ , and M (M'). (f) Color plot of the \mathbb{Z}_4 Berry phase. (g) Schematic figures for two limits for $(\delta t, \delta\gamma) = (1, 1/2)$, $(\delta t, \delta\gamma) \neq (\pm 1, \pm 1/2)$ and $(\delta t, \delta\gamma) = (-1, -1/2)$.

$$h(\vec{k}) = \begin{pmatrix} q_{2 \times 2}(-k_y, k_y) & q_{2 \times 2}(k_x, k_x) \\ q_{2 \times 2}(-k_x, -k_x) & q_{2 \times 2}(k_y, -k_y) \end{pmatrix}, \quad (2)$$

with

$$q_{2 \times 2}(k_1, k_2) = \begin{pmatrix} 0 & t_1 - \gamma_1 + (t_2 - \gamma_2)e^{ik_1} \\ t_1 + \gamma_1 + (t_2 + \gamma_2)e^{ik_2} & 0 \end{pmatrix}. \quad (3)$$

This bulk Hamiltonian preserves the generalized four-fold rotational symmetry,

$$U_4 h(\vec{k}) U_4^{-1} = h^\dagger(R_4 \vec{k}), \quad (4)$$

with

$$R_4 = \begin{pmatrix} 0 & -1 \\ 1 & 0 \end{pmatrix}, \quad (5)$$

and U_4 being a unitary operator

$$U_4 = \begin{pmatrix} 0 & 0 & 0 & 1 \\ 1 & 0 & 0 & 0 \\ 0 & 1 & 0 & 0 \\ 0 & 0 & 1 & 0 \end{pmatrix}. \quad (6)$$

The eigenvalues E_i ($i = 1, \dots, 4$) of $h(\vec{k})$ are

$$\begin{aligned} E_1(\vec{k}) &= -a(\vec{k}) + \sqrt{b(\vec{k})}, & E_2(\vec{k}) &= a(\vec{k}) + \sqrt{b(\vec{k})}, \\ E_3(\vec{k}) &= -a(\vec{k}) - \sqrt{b(\vec{k})}, & E_4(\vec{k}) &= a(\vec{k}) - \sqrt{b(\vec{k})}, \end{aligned} \quad (7)$$

with

$$\begin{aligned} a(\vec{k}) &= t_1^2 + t_2^2 - \gamma_1^2 - \gamma_2^2 + (t_1 t_2 - \gamma_1 \gamma_2)(\cos k_x + \cos k_y), \quad (8) \\ b(\vec{k}) &= -(t_1 - \gamma_1)(t_1 + \gamma_1)(t_2 - \gamma_2)(t_2 + \gamma_2)(\cos k_x - \cos k_y)^2 \\ &\quad + (t_1^2 + t_2^2 - \gamma_1^2 - \gamma_2^2 + (t_1 t_2 - \gamma_1 \gamma_2)(\cos k_x + \cos k_y))^2. \quad (9) \end{aligned}$$

For the following discussions, we introduce δt and $\delta\gamma$ as

$$t_1 = 1 + \delta t, \quad t_2 = 1 - \delta t, \quad (10)$$

$$\gamma_1 = \frac{1}{2} + \delta\gamma, \quad \gamma_2 = \frac{1}{2} - \delta\gamma. \quad (11)$$

In Figs. 1 (b)-(d), the energy spectrum of the bulk Hamiltonian in Eq. (2) is plotted for $(\delta t, \delta\gamma) = (-0.7, 0.1)$, $(0, 0.1)$ and $(0.7, 0.1)$. There are real line gaps along the line $k_x = k_y$ for $-\delta t < \delta\gamma < \delta t$.

\mathbb{Z}_4 Berry Phase Protected by Generalized Four-Fold Rotational Symmetry: We see the topological invariant to characterize the real line gap topology. Specifically, we introduce the \mathbb{Z}_4 Berry phase protected by generalized four-fold symmetry in a two-dimensional momentum space. The key idea originates from the quantized Berry phase protected by the crystalline symmetry.^{16, 18, 24, 81, 112–114, 116} In addition, the notion of the complex Berry phase also plays an important role.^{35, 45, 81, 131, 132} Furthermore, in the presence of the crystalline symmetry, the form of the topological invariant can be simplified to one determined from the data at high-symmetry points in the Brillouin zone. This reduction is important from the view of the computational costs.

In this paper, we consider the topology of the bands at the left side of the real line gap. The \mathbb{Z}_4 Berry phase is defined as follows. Firstly, we define the $n_{\text{occ}} \times n_{\text{occ}}$ Berry connection as

$$\vec{A}(\vec{k}) = -i \Phi^\dagger(\vec{k}) \frac{\partial}{\partial \vec{k}} \Psi(\vec{k}), \quad (12)$$

where

$$\Psi(\vec{k}) = (\vec{\psi}_1(\vec{k}), \dots, \vec{\psi}_{n_{\text{occ}}}(\vec{k})), \quad (13)$$

and

$$\Phi(\vec{k}) = (\vec{\phi}_1(\vec{k}), \dots, \vec{\phi}_{n_{\text{occ}}}(\vec{k})), \quad (14)$$

denote right and left eigenvectors in the momentum space,

respectively. Here, n_{occ} is the number of the occupied states. The \mathbb{Z}_4 Berry phase in the non-Hermitian system is

$$\nu = \text{Tr} \int_L \frac{d\vec{k}}{2\pi} \cdot \vec{A}(\vec{k}), \quad (15)$$

where L denotes the paths between the high-symmetry points in the Brillouin zone [see Fig. 1 (e)].

To evaluate Eq. (15), we consider the constraints on the eigenvectors and the Berry connection arising from the presence of generalized four-fold symmetry. In the presence of generalized four-fold symmetry, the constraints on the right and left eigenvectors are

$$\Psi'(\vec{k}) = U_4 \Phi(R_4^{-1} \vec{k}) \Theta(R_4^{-1} \vec{k}) \quad (16)$$

$$\Phi'(\vec{k}) = U_4 \Psi(R_4^{-1} \vec{k}) \Theta(R_4^{-1} \vec{k}) \quad (17)$$

where $\Theta(\vec{k}) = \text{diag}(e^{i\theta_1(\vec{k})}, \dots, e^{i\theta_{n_{\text{occ}}}(\vec{k})})$ is the $n_{\text{occ}} \times n_{\text{occ}}$ matrix. Here, the explicit forms of $\Psi'(\vec{k})$ and $\Phi'(\vec{k})$ are

$$\Psi'(\vec{k}) = (\vec{\psi}_1(\vec{k}), \dots, \vec{\psi}_{n_{\text{occ}}}(\vec{k})), \quad (18)$$

$$\Phi'(\vec{k}) = (\vec{\phi}_1(\vec{k}), \dots, \vec{\phi}_{n_{\text{occ}}}(\vec{k})), \quad (19)$$

where j^* ($j = 1, \dots, n_{\text{occ}}$) denotes the index with $E_{j^*}(\vec{k}) = (E_j(\vec{k}))^* = E_j(R_4^{-1} \vec{k})$. From the assumption of the presence of the real line gap, the following holds: if the band with the index j is at the left side of the real line gap, so is the band with the index j^* . This indicates that there exist $\psi_j(\vec{k})$ ($\phi_j(\vec{k})$) and $\psi_{j^*}(\vec{k})$ ($\phi_{j^*}(\vec{k})$) as elements of the column vector $\Psi'(\vec{k})$ ($\Phi'(\vec{k})$).

From these constraints on the eigenvectors, the Berry connection satisfies

$$\begin{aligned} \mathbf{A}(\vec{k}) = & -i\Theta^{-1}(R_4^{-1} \vec{k}) \left\{ (\Psi'(R_4^{-1} \vec{k}))^\dagger \frac{\partial}{\partial \vec{k}} \Phi'(R_4^{-1} \vec{k}) \right\} \Theta(R_4^{-1} \vec{k}) \\ & - i\Theta^{-1}(R_4^{-1} \vec{k}) \frac{\partial}{\partial \vec{k}} \Theta(R_4^{-1} \vec{k}). \end{aligned} \quad (20)$$

By making use of Eq. (20), we obtain

$$\text{Re } \nu = \frac{1}{2\pi} \sum_{i \leq n_{\text{occ}}} (\theta_i(M) - \theta_i(\Gamma)) = \frac{n}{4} \pmod{1}, \quad (21)$$

where n is 0, 1, 2, or 3. Here, from Eq. (17) and the biorthogonal normalization condition $\phi_i^*(\vec{k}') \psi_i(\vec{k}) = \delta_{i' i} \delta(\vec{k}' - \vec{k})$, the explicit form of $\theta_i(\vec{k})$ is

$$\theta_i(\vec{k}) = -\arg((\vec{\psi}_i(R_4 \vec{k}))^\dagger U_4 \vec{\psi}_i(\vec{k})). \quad (22)$$

The detailed derivation of Eq. (21) is presented in Supplemental Materials. We note that even if there are the exceptional points on the path L except the high-symmetry points Γ and M in Fig. 1 (e), we can avoid them by the continuous deformation of the integration path. This is the unique advantage of employing the \mathbb{Z}_4 Berry phase, since the topological invariant such that the Chern number can not be defined when there exists an exceptional point in the two-dimensional Brillouin zone.

We further show the explicit computation of the \mathbb{Z}_4 Berry phase for the present model. We note that we focus on the real line gap at the red line in Figs. 1 (b) and (d). At the high symmetry points Γ and M , the explicit forms of the right eigenvectors of E_1 which are the isolated energy spectrum at the

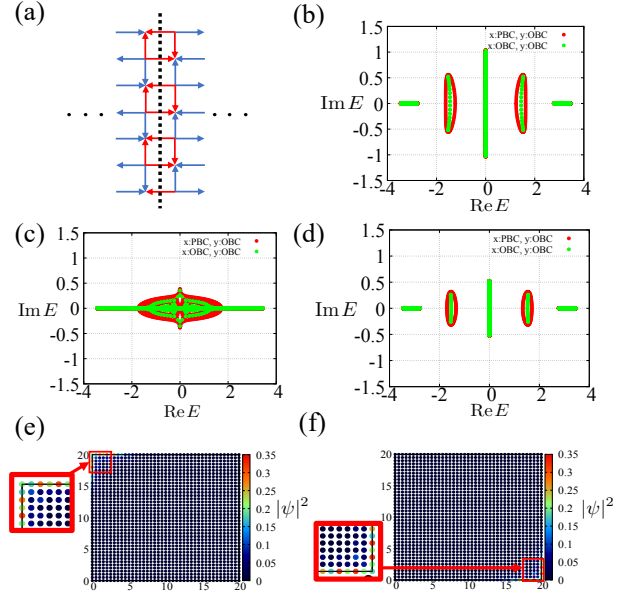


Fig. 2. (Color online) (a) Schematic figure for the boundary shape of the two-dimensional SSH model with nonreciprocal hoppings when considering the cylinder geometry. We arrange to break the inversion symmetry. The dashed line shows the center of the generalized mirror plane. (b)-(d) The red (green) dots show the energy spectrum under the periodic (open) boundary condition along the x direction. For several parameters sets of $(\delta t, \delta \gamma)$, (b), (c), and (d) show the data for $(\delta t, \delta \gamma) = (-0.7, 0.1)$, $(0, 0.1)$, and $(0.7, 0.1)$, respectively. (e) and (f) show the distribution of the right eigenvector in the real space of corner states for $(\delta t, \delta \gamma, E) = (-0.7, 0.1, -1.51302 + 0.480218i)$ and $(0.7, 0.1, -1.54824 + 0.260155i)$, respectively.

left side in Fig. 1 (a) are

$$\vec{\psi}_1(\Gamma) = \left(-\frac{1}{2\sqrt{3}}, \frac{1}{2}, -\frac{1}{2\sqrt{3}}, \frac{1}{2} \right)^T, \quad (23)$$

$$\vec{\psi}_1(M) = \left(-\frac{\sqrt{\delta t^2 - \delta \gamma^2}}{2(\delta t - \delta \gamma)}, \frac{1}{2}, -\frac{\sqrt{\delta t^2 - \delta \gamma^2}}{2(\delta t - \delta \gamma)}, \frac{1}{2} \right)^T, \quad (24)$$

respectively. Thus, the explicit forms of $\theta_1(\vec{k})$ at Γ and M are

$$\theta_1(\Gamma) = -\arg\left(-\frac{1}{\sqrt{3}}\right), \quad \theta_1(M) = -\arg\left(-\frac{\sqrt{\delta t^2 - \delta \gamma^2}}{\delta t - \delta \gamma}\right). \quad (25)$$

In Fig. 1 (f), we show the color map of \mathbb{Z}_4 phase of the band $E_1(\vec{k})$ in Eq. (21). The \mathbb{Z}_4 Berry phase takes values of $\text{Re } \nu = 1/2$ (yellow area) and $\text{Re } \nu = 0$ (blue area). The white area shows the existence of the exceptional rings around the high-symmetry point M .

Before closing this discussion, we address the adiabatic connection of the \mathbb{Z}_4 Berry phase. Since the \mathbb{Z}_4 Berry phase does not change as long as the real line gap is closed, the system can be adiabatically deformed into a certain limit that has the same Berry phase. In the present model, the phase with $\text{Re } \nu = 0$ is connected to the limit of $\delta t = 1$ and $\delta \gamma = 1/2$ [see Fig. 1 (g)], while the phase with $\text{Re } \nu = 1/2$ is connected to the limit of $\delta t = -1$ and $\delta \gamma = -1/2$ [see Fig. 1 (g)]. This insight is essential to understand the relation between edge states and the \mathbb{Z}_4 Berry phase.

Edge Spectrum on the Cylinder Geometry: Before going

to the numerical result of the edge spectra, to get the insight of the relation between the \mathbb{Z}_4 Berry phase and edge states, we consider the two limits, i.e., $(\delta t, \delta \gamma) = (1, 1/2)$ and $(\delta t, \delta \gamma) = (-1, -1/2)$. For $(\delta t, \delta \gamma) = (1, 1/2)$, there exist dimers on the right and bottom sides, while there exist dimers on the left and top sides for $(\delta t, \delta \gamma) = (-1, -1/2)$. By combining with the discussion of the adiabatic connection of the \mathbb{Z}_4 Berry phase, $\text{Re } \nu = 1/2$ (0) predicts the emergence of the edge states at left and top (right and bottom) sides. Thus, the \mathbb{Z}_4 Berry phase indicates the position of edge states.

Once the profile of edge states are understood by the \mathbb{Z}_4 Berry phase, we can then argue the characterization of the skin effect of the edge spectra. To be more concrete, the non-zero winding number of the edge spectrum provides the emergence of the hybrid higher-order topological skin modes. The explicit form of the winding number of the edge spectra is

$$w = \int_{-\pi}^{\pi} \frac{dk}{2\pi i} \frac{\partial}{\partial k} \log \det(h_{1D}(k) - E_{\text{ref}}), \quad (26)$$

where $h_{1D}(k)$ denotes the Hamiltonian on the cylinder geometry. However, in the presence of the conventional inversion symmetry [see Eq. (4)], the total of the winding number vanishes.⁷⁵⁾ To avoid this problem, we consider the system in the absence of inversion symmetry by setting the appropriate edges [see Fig. 2 (a)]. The trivial case of edge spectra is discussed in Supplemental materials.

We note that, in the present model, we can also define \mathbb{Z}_2 indicator with generalized mirror symmetry that predicts the emergence of the skin effect and hybrid higher-order topological skin modes⁷⁵⁾ [see Fig. 2 (a)]. The detail is discussed in Supplemental materials.

Figures 2 (b), (c), and (d) display energy spectra under the periodic (open) boundary condition along x (y) direction for $(\delta t, \delta \gamma) = (-0.7, 0.1)$, $(0, 0.1)$, and $(0.7, 0.1)$, respectively. Here, we set the number of the unit cells as 20. Thus, the total number of the lattice sites are 82. There exists the energy spectrum of edge states where eigenvectors are localized at top and left [bottom and right] side for $(\delta t, \delta \gamma) = (-0.7, 0.1)$ [(0.7, 0.1)]. Here, we note that there may exist the energy spectrum of edge states even in the presence of gapless states. Thus, the emergence of all edge states are not predicted by the \mathbb{Z}_4 Berry phase.

Localized States at the Corner: Finally, we demonstrate that the system hosts corner skin modes. We consider the 1681-site system with the open boundary condition in both directions [see Fig. 2 (a)]. In Figs. 2 (c) and (d), we see the emergence of the corner skin modes arising from the edge states at the left top (right bottom) corner for $\delta t = -0.7$ and 0.7 [see Figs. 2 (e) and (f)].

Combining the above numerical result and the topological invariants, we conclude that the following bulk-boundary correspondence between the pair of topological number $(\text{Re } \nu, w)$ and the hybrid higher-order topological skin modes holds. Specifically, $(\text{Re } \nu, w) = (1/2, -1)$ indicates the emergence of the hybrid higher-order topological skin modes at the left top corner, while $(\text{Re } \nu, w) = (0, 1)$ indicates the emergence of the hybrid higher-order topological skin modes at the right bottom corner. This correspondence between the topological invariants and hybrid higher-order topological skin modes originates from the physical picture of the adiabatic connection.

Summary: We have realized the hybrid higher-order topo-

logical skin modes in two-dimensional SSH model with non-reciprocal hoppings. Specifically, we characterize the real line gap topology by introducing the \mathbb{Z}_4 Berry phase protected by generalized four-fold rotational symmetry. Additionally, from the discussion of the adiabatic connection, we show the relation between the position of edge states and the topological invariant. Moreover, from the nontrivial point gap arising by the edge spectra, we demonstrate that the present model hosts the localized states at the corner. In particular, the position of these localized states are predicted by the pair of the \mathbb{Z}_4 Berry phase and the winding number.

Acknowledgment: The author thanks T. Mizoguchi for fruitful discussions. This work is supported by JST, the establishment of university fellowships towards the creation of science technology innovation, Grant No. JPMJFS2106.

- 1) Y. Hatsugai, Phys. Rev. Lett. **71**, 3697 (1993).
- 2) Y. Hatsugai, Phys. Rev. B **48**, 11851 (1993).
- 3) C. L. Kane and E. J. Mele, Phys. Rev. Lett. **95**, 146802 (2005).
- 4) J. C. Y. Teo, L. Fu, and C. L. Kane, Phys. Rev. B **78**, 045426 (2008).
- 5) X.-L. Qi, T. L. Hughes, and S.-C. Zhang, Phys. Rev. B **78**, 195424 (2008).
- 6) M. Z. Hasan and C. L. Kane, Rev. Mod. Phys. **82**, 3045 (2010).
- 7) X.-L. Qi and S.-C. Zhang, Rev. Mod. Phys. **83**, 1057 (2011).
- 8) M. Sato and S. Fujimoto, J. Phys. Soc. Jpn. **85**, 072001 (2016).
- 9) L. Fu and C. L. Kane, Phys. Rev. B **74**, 195312 (2006).
- 10) L. Fu, C. L. Kane, and E. J. Mele, Phys. Rev. Lett. **98**, 106803 (2007).
- 11) J. E. Moore and L. Balents, Phys. Rev. B **75**, 121306(R) (2007).
- 12) H. Zhang, C.-X. Liu, X.-L. Qi, X. Dai, Z. Fang, and S.-C. Zhang, Nat. Phys. **5**, 438 (2009).
- 13) R. Roy, Phys. Rev. B **79**, 195322 (2009).
- 14) D. Hsieh, Y. Xia, D. Qian, L. Wray, F. Meier, J. H. Dil, J. Osterwalder, L. Patthey, A. V. Fedrov, H. Lin, A. Bansil, D. Grauer, Y. S. Hor, R. J. Cave, and M. Z. Hasan, Phys. Rev. Lett. **103**, 146401 (2009).
- 15) C.-K. Chiu, J. C. Y. Teo, A. P. Schnyder, and S. Ryu, Rev. Mod. Phys. **88**, 035005 (2016).
- 16) J. Zak, Phys. Rev. Lett. **62**, 2747 (1989).
- 17) L. Fu, Phys. Rev. Lett. **106**, 106802 (2011).
- 18) Y. Hatsugai and I. Maruyama, Europhys. Lett. **95** 20003 (2011).
- 19) C. Fang, M. J. Gilbert, and B. A. Bernevig, Phys. Rev. B **86**, 115112 (2012).
- 20) R.-J. Slager, A. Mesaros, V. Juričić, and J. Zaanen, Nat. Phys. **9**, 98 (2013).
- 21) Y. Kim, B. J. Wieder, C. L. Kane, and A. M. Rappe, Phys. Rev. Lett. **115**, 036806 (2015).
- 22) H. C. Po, A. Vishwanath, and H. Watanabe, Nat. Commun. **8**, 1 (2017).
- 23) J. Kruthoff, J. de Boer, E. J. van Wezel, C. L. Kane, and R.-J. Skager, Phys. Rev. X **7**, 041069 (2017).
- 24) T. Kariyado, T. Morimoto, and Y. Hatsugai, Phys. Rev. Lett. **120**, 247202 (2018).
- 25) S. Ono and H. Watanabe, Phys. Rev. B **98**, 115150 (2018).
- 26) H. Watanabe, and L. Lu, Phys. Rev. Lett. **121**, 263903 (2018).
- 27) N. Hatano and D. R. Nelson, Phys. Rev. Lett. **77**, 570 (1996).
- 28) C. M. Bender and S. Boettcher, Phys. Rev. Lett. **80**, 5243 (1998).
- 29) I. Rotter, J. Phys. A **42**, 153001 (2009).
- 30) M. Sato, K. Hasebe, K. Esaki, and M. Kohmoto, Prog. Theor. Phys. **127**, 937 (2012).
- 31) Y. Ashida, S. Furukawa, and M. Ueda, Phys. Rev. A **94**, 053615 (2016).
- 32) Y. Adhida, S. Furukawa, and M. Ueda, Nat. Commun. **8**, 15791 (2017).
- 33) Y. C. Hu and T. L. Hughes, Phys. Rev. B **84**, 153101 (2011).
- 34) K. Esaki, M. Sato, K. Hasebe, and M. Kohmoto, Phys. Rev. B **84**, 2051128 (2011).
- 35) S.-D. Liang and G.-Y. Huang, Phys. Rev. A **87**, 012118 (2013).
- 36) Z. Gong, S.-Higashikawa, and M. Ueda, Phys. Rev. Lett. **118**, 200401 (2017).
- 37) H. Shen, B. Zhen, and L. Fu, Phys. Rev. Lett. **120**, 146402 (2018).

- 38) S. Yao, F. Song, and Z. Wang Phys. Rev. Lett. **121**, 136802 (2018).
- 39) Z. Gong, Y. Ashida, K. Kawabata, K. Takasan, S. Higashikawa, and M. Ueda, Phys. Rev. X **8**, 031079 (2018).
- 40) J. Carlström and E. J. Bergholtz, Phys. Rev. A **98**, 042114 (2018).
- 41) J. Carlström, M. Stålhammar, J. C. Budich, and E. J. Bergholtz, Phys. Rev. B **99**, 161115(R) (2019).
- 42) N. Okuma and M. Sato, Phys. Rev. Lett. **123**, 097701 (2019).
- 43) T. Yoshida, K. Kudo, Y. Hatsugai, Sci. Rep. **9**, 16895 (2019).
- 44) K. Kawabata, K. Shiozaki, M. Ueda, and M. Sato, Phys. Rev. X **9**, 041015 (2019).
- 45) S. Longhi and L. Feng, Phys. Rev. B **107**, 085122 (2023).
- 46) N. Okuma, M. Sato, Annu. Rev. Condens. Matter Phys. **13**, 83 (2023).
- 47) F. K. Kunst, E. Edvardsson, J. C. Budich, and E. J. Bergholtz, Phys. Rev. Lett. **121**, 026808 (2018).
- 48) S. Yao, and Z. Wang, Phys. Rev. Lett. **121**, 086803 (2018).
- 49) C. H. Lee and R. Thomale, Phys. Rev. B **99**, 201103(R) (2019).
- 50) D. S. Borgnia, A. J. Kruchkov, and R.-J. Slager, Phys. Rev. Lett. **124**, 056802 (2020).
- 51) K. Zhang, Z. Yang, and C. Fang, Phys. Rev. Lett. **125**, 126402 (2020).
- 52) N. Okuma, K. Kawabata, K. Shiozaki, and M. Sato, Phys. Rev. Lett. **124**, 086801 (2020).
- 53) N. Okuma, M. Sato, Phys. Rev. Lett. **126**, 176601 (2021).
- 54) X.-Q. Sun, P. Zhu, and T. L. Hughes, Phys. Rev. Lett. **127**, 066401 (2021).
- 55) R. Lin, T. Tai, L. Li, C. H. Lee, Front. Phys. **18**, 53605, (2023).
- 56) T. Yoshida, S.-B. Zhang, T. Neupert, N. Kawakami, arXiv:2309.14111.
- 57) B. Zhen, C. W. Hsu, Y. Igarashi, L. Lu, I. Kaminer, A. Pick, S.-L. Chua, J. D. Joannopoulos, and M. Soljačić, Nature (London) **525**, 354 (2015).
- 58) T. E. Lee, Phys. Rev. Lett. **116**, 133903 (2016).
- 59) D. Leykam, K. Y. Bliokh, C. Huang, Y. D. Chong, and F. Nori, Phys. Rev. Lett. **118**, 040401 (2017).
- 60) V. Kozii and L. Fu, arXiv:1708.05841.
- 61) V. M. Martinez Alvarez, J. E. Barrios Vargas, and L. E. F. Foa Torres Phys. Rev. B **97**, 121401(R) (2018).
- 62) T. Yoshida, R. Peters, and N. Kawakami, Phys. Rev. B **98**, 035141 (2018).
- 63) K. Kawabata, T. Bessho, and M. Sato, Phys. Rev. Lett. **123**, 066405 (2019).
- 64) C. C. Wojcik, X.-Q. Sun, T. Bzdušek, and S. Fan, Phys. Rev. B **101**, 205417 (2020).
- 65) E. J. Bergholtz, J. C. Budich, and F. K. Kunst, Rev. Mod. Phys. **93**, 015005 (2021).
- 66) Z. Yang, A. P. Schnyder, J. Hu, and C.-K. Chiu, Phys. Rev. Lett. **126**, 086401 (2021).
- 67) W. B. Rui, Z. Zheng, C. Wang, and Z. D. Wang, Phys. Rev. Lett. **128**, 226401 (2022).
- 68) J. C. Budich, J. Carlström, F. K. Kunst, and E. J. Bergholtz, Phys. Rev. B **99**, 041406(R) (2019).
- 69) R. Okugawa, and T. Yokoyama, Phys. Rev. B **99**, 041202(R) (2019).
- 70) H. Zhou, J. Y. Lee, S. Liu, and B. Zhen, Optica **6**, 190 (2019).
- 71) C.-H. Liu, H. Jiang, and S. Chen, Phys. Rev. B **99**, 125103 (2019).
- 72) T. Yoshida, R. Peters, N. Kawakami, and Y. Hatsugai, Phys. Rev. B **99**, 121101(R) (2019).
- 73) H. Zhou and J. Y. Lee, Phys. Rev. B **99**, 235112 (2019).
- 74) T. Yoshida, T. Mizoguchi, and Y. Hatsugai, Phys. Rev. Research **2**, 022062(R) (2020).
- 75) R. Okugawa, R. Takahashi, and K. Yokomizo, Phys. Rev. B **103**, 205205 (2021).
- 76) P. M. Vecsei, M. M. Denner, T. Neupert, and F. Schindler, Phys. Rev. B **103**, L201114 (2021).
- 77) K. Shiozaki and S. Ono, Phys. Rev. B **104**, 035424, (2021).
- 78) I. Mandal, E. J. Bergholtz, Phys. Rev. Lett. **127**, 186601 (2021).
- 79) P. Delplace, T. Yoshida, and Y. Hatsugai, Phys. Rev. Lett. **127**, 186602 (2021).
- 80) K. Chen and A. B. Khanikaev, Phys. Rev. B **105**, L081112 (2022).
- 81) S. Tsubota, H. Yang, Y. Akagi, and H. Katsura, Phys. Rev. B **105**, L201113 (2022).
- 82) T. Yoshida, R. Okugawa, and Y. Hatsugai, Phys. Rev. B **105**, 085109 (2022).
- 83) H. Wakao, T. Yoshida, and Y. Hatsugai, Phys. Rev. B **105**, 214103 (2022).
- 84) Y. Tanaka, R. Takahashi, R. Okugawa, arXiv:2306.08923.
- 85) Y. Xu, S.-T. Wang, and L.-M. Duan, Phys. Rev. Lett. **118**, 045701 (2017).
- 86) T. Yoshida, K. Kudo, H. Katsura, and Y. Hatsugai, Phys. Rev. Research **2**, 033428 (2020).
- 87) M. Ezawa, Phys. Rev. B **99**, 201411(R) (2019).
- 88) T. Hofmann, T. Helbig, C. H. Lee, M. Greiter, and R. Thomale, Phys. Rev. Lett. **122**, 247702 (2019).
- 89) M. Ezawa, Phys. Rev. B **100**, 081401 (2019).
- 90) T. Helbig, T. Hofmann, S. Imhof, M. Abdelghany, T. Kiessling, L. W. Molenkamp, C. H. Lee, A. Szameit, M. Greiter, and R. Thomale, Nat. Phys. **16**, 747 (2020).
- 91) T. Hofmann, T. Helbig, F. Schindler, N. Salgo, M. Brezińska, M. Greiter, T. Kiessling, D. Wolf, A. Vollhardt, A. Kabašić, C. H. Lett, A. Bilišić, R. Thomale, and T. Neupert, Phys. Rev. Research **2**, 023265 (2020).
- 92) T. Yoshida and Y. Hatsugai, Phys. Rev. B **100**, 054109 (2019).
- 93) A. Ghatak, M. Brandenbourger, J. van Wesel, and C. Coullais, Proc. Natl. Acad. Sci. USA **117**, 29561 (2020).
- 94) C. Scheibner, W. T. M. Irvine, and V. Vitelli, Phys. Rev. Lett. **125**, 118001 (2020).
- 95) A. Guo, G. J. Salamo, D. Duchesne, R. Morandotti, M. Volatier-Ravat, V. Aimez, G. A. Siviloglou, and D. N. Christodoulides, Phys. Rev. Lett. **103**, 093902 (2009).
- 96) C. E. Rüter, K. G. Makris, R. El-Ganainy, D. N. Christodoulides, M. Segev, and D. Kip, Nat. Phys. **6**, 192 (2010).
- 97) L. Feng, R. El-Ganainy, and L. Ge, Nat. Photonics **11**, 752 (2017).
- 98) T. Isobe, T. Yoshida, and Y. Hatsugai, Phys. Rev. B **104**, L121105 (2021).
- 99) W. A. Benalcazar, B. A. Bernevig, and T. L. Hughes, Science **357**, 61 (2017).
- 100) W. A. Benalcazar, B. A. Bernevig, and T. L. Hughes, Phys. Rev. B **96**, 245115 (2017).
- 101) M. Ezawa, Phys. Rev. Lett. **120**, 026801 (2018).
- 102) F. Schindler, A. M. Cook, M. G. Vergniory, Z. Wang, S. S. P. Parkin, B. A. Bernevig, and T. Neupert, Sci. Adv. **4**, eaat0346 (2018).
- 103) F. K. Kunst, G. van Miert, and E. J. Bergholtz, Phys. Rev. B **97**, 241405(R) (2018).
- 104) F. Schindler, Z. Wang, M. G. Vergniory, A. M. Cook, A. Murani, S. Sengupta, A. Y. Kasumov, R. Deblock, S. Jeon, I. Drozdov, H. Bouchiat, S. Guéron, A. Yazdani, B. A. Bernevig, and T. Neupert, Nat. Phys. **14**, 918 (2018).
- 105) S. Hayashi, Commun. Math. Phys. **364**, 343 (2018).
- 106) R. Okugawa, S. Hayashi, and T. Nakanishi, Phys. Rev. B **100**, 235302 (2019).
- 107) Z. Song, Z. Fang, and C. Fang, Phys. Rev. Lett. **119**, 246402 (2017).
- 108) E. Khalaf, Phys. Rev. B **97**, 205136 (2018).
- 109) A. Matsugatani and H. Watanabe, Phys. Rev. B **98**, 205129 (2018).
- 110) L. Trifunovic and P. W. Brouwer, Phys. Rev. X **9**, 011012 (2019).
- 111) W. A. Benalcazar, T. Li, and T. L. Hughes Phys. Rev. B **99**, 245151 (2019).
- 112) T. Mizoguchi, H. Araki, and Y. Hatsugai, J. Phys. Soc. Jpn. **88**, 104703 (2019).
- 113) K. Kudo, T. Yoshida, and Y. Hatsugai, Phys. Rev. Lett. **123**, 196402 (2019).
- 114) H. Araki, T. Mizoguchi, and Y. Hatsugai, Phys. Rev. Research **2**, 012009(R) (2020).
- 115) R. Takahashi, Y. Tanaka, and S. Murakami, Phys. Rev. Research **2**, 013300 (2020).
- 116) H. Wakao, T. Yoshida, H. Araki, T. Mizoguchi, and Y. Hatsugai, Phys. Rev. B **101**, 94107 (2021).
- 117) T. Liu, Y.-R. Zhang, Q. Ai, Z. Gong, K. Kawabata, M. Ueda, and F. Nori, Phys. Rev. Lett. **122**, 076801 (2019).
- 118) E. Edvardsson, F. K. Kunst, and E. J. Bergholtz, Phys. Rev. B **99**, 081302(R) (2019).
- 119) X.-W. Luo and C. Zhang, Phys. Rev. Lett. **123**, 073601 (2019).
- 120) Y. Yu, M. Jung, and G. Shvets, Phys. Rev. B **103**, L041102 (2021).
- 121) C. H. Lee, and L. Li, and J. Gong, Phys. Rev. Lett. **123**, 016805 (2019).
- 122) X. Zhang, Y. Tian, J.-H. Jiang, M.-H. Lu, and Y.-F. Chen, Nat. Commun. **12**, 5377 (2021).
- 123) D. Zou, T. Chen, W. He, J. Bao, C. H. Lee, H. Sun, and X. Zhang, Nat. Commun. **12**, 7201 (2021).
- 124) Y. Li, C. Liang, C. Wang, C. Lu, and Y. Liu, Phys. Rev. Lett. **128**, 223903 (2022).

- 125) W. Zhu and J. Gong, Phys. Rev. B **106**, 035425 (2022).
- 126) W. Zhu and J. Gong, Phys. Rev. B **108**, 035406, (2023).
- 127) J. Sun, C.-A. Li, Si. Feng, and H. Guo, Phys. Rev. B **108**, 075122 (2023).
- 128) K. Kawabata, M. Sato, and K. Shiozaki, Phys. Rev. B **102**, 205118 (2020).
- 129) R. Okugawa, R. Takahashi, and K. Yokomizo, Phys. Rev. B **102**, 241202(R) (2020).
- 130) Y. Fu, J. Hu, and S. Wan, Phys. Rev. B **103**, 045420 (2021).
- 131) J. Garrison and E. M. Wright, Phys. Lett. A **128**, 177 (1988).
- 132) C. Miniatura, C. Sire, J. Baudon, and J. Bellissard, Europhys. Lett. **13**, 199 (1990).

Supplemental Material for “Hybrid Higher-Order Topological Skin Modes in the Two-Dimensional Su–Schrieffer–Heeger Model with Nonreciprocal Hoppings”

Hiromasa Wakao

Graduate School of Pure and Applied Sciences, University of Tsukuba, Tsukuba, Ibaraki 305-8571, Japan

(Dated: December 4, 2023)

I. CONSTRAINTS ON THE EIGENVECTORS AND THE BERRY CONNECTION BY GENERALIZED FOUR-FOLD ROTATIONAL SYMMETRY

Here, we show the details of the constraint on the eigenvectors and the Berry connection arising from the presence of generalized four-fold rotational symmetry. First, we consider the constraints from generalized four-fold rotational symmetry [1, 2]. From the constraint on the Hamiltonian, the eigenvalue equation is rewritten as

$$\begin{aligned} H(\vec{k})\psi_n(\vec{k}) &= E_n(\vec{k})\psi_n(\vec{k}) \\ H^\dagger(R_4\vec{k})U_4\psi_n(\vec{k}) &= E_n(\vec{k})U_4\psi_n(\vec{k}), \end{aligned} \quad (\text{S.1})$$

with n being the band index. Thus, the constraint on the right eigenvectors are

$$\phi_{j^*}(R_4\vec{k}) = e^{i\theta_j(\vec{k})}U_4\psi_j(\vec{k}). \quad (\text{S.2})$$

By the same approach, we also obtain the constraint on the left eigenvectors

$$\psi_{j^*}(R_4\vec{k}) = e^{i\theta_j(\vec{k})}U_4\phi_j(\vec{k}). \quad (\text{S.3})$$

Here, the phase factor in Eq. (S.3) is determined from the biorthogonal normalization condition $\phi_j^*(\vec{k}')\psi_{j'}(\vec{k}) = \delta_{jj'}\delta(\vec{k} - \vec{k}')$. Thus, we obtain the relation in Eqs. (16) and (17).

Second, we show the relation in Eq. (20). From the constraints on the eigenvectors, the Berry connection is rewritten as

$$\begin{aligned} \vec{A}(\vec{k}) &= -i \left\{ \Theta^{-1}(R_4^{-1}\vec{k})(\Psi')^\dagger(R_4^{-1}\vec{k})U_4^{-1} \right\} \frac{\partial}{\partial \vec{k}} \left\{ U_4 \Phi'(R_4^{-1}\vec{k})\Theta(R_4^{-1}\vec{k}) \right\} \\ &= -i\Theta^{-1}(R_4^{-1}\vec{k}) \left((\Psi')^\dagger(R_4^{-1}\vec{k}) \frac{\partial}{\partial \vec{k}} \Phi'(R_4^{-1}\vec{k}) \right) \Theta(R_4^{-1}\vec{k}) - i\Theta^{-1}(R_4^{-1}\vec{k}) \frac{\partial}{\partial \vec{k}} \Theta(R_4^{-1}\vec{k}). \end{aligned} \quad (\text{S.4})$$

Thus, we obtain Eq. (18) of the main text.

II. QUANTIZATION OF THE BERRY PHASE WITH GENERALIZED FOUR-FOLD ROTATIONAL SYMMETRY

We show the details of the quantization of the Berry phase. In order to show the \mathbb{Z}_4 quantization of $\text{Re}\nu$, we consider the sum of the Berry phase defined as a contour integral along four paths (L_1 - L_4) in Fig. 1,

$$\nu_{\text{all}} = \sum_{i=1}^4 \nu_i, \quad (\text{S.5})$$

with

$$\nu_i = \text{Tr} \int_{L_i} \frac{d\vec{k}}{2\pi} \cdot \vec{A}(\vec{k}). \quad (\text{S.6})$$

Here, the path L_i connect high-symmetry points in Fig. 1. We note that L_1 is identical to L in Eq. (15). Since ν_{all} is the closed path, $\nu_{\text{all}} = n'$ where n' is an integer. From the constraints on the Berry connection, ν_2 can be rewritten

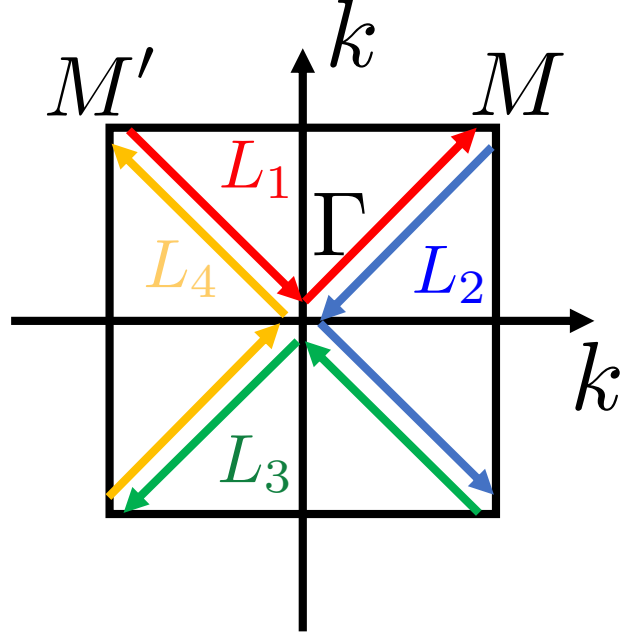


Fig. 1. (Color online) Sketch of the Brillouin zone and the path of the integration in Eq. (S.6).

into

$$\begin{aligned}
\nu_2 &= \text{Tr} \int_{L_2} \frac{d\vec{k}}{2\pi} \cdot \left\{ -i\Theta^{-1}(R_4^{-1}\vec{k}) \left((\Psi')^\dagger(R_4^{-1}\vec{k}) \frac{\partial}{\partial \vec{k}} \Phi'(R_4^{-1}\vec{k}) \right) \Theta(R_4^{-1}\vec{k}) - i\Theta^{-1}(R_4^{-1}\vec{k}) \frac{\partial}{\partial \vec{k}} \Theta(R_4^{-1}\vec{k}) \right\} \\
&= \text{Tr} \int_{L_2} \frac{d\vec{k}}{2\pi} \cdot \left\{ -i \left(\Psi^\dagger(R_4^{-1}\vec{k}) \frac{\partial}{\partial \vec{k}} \Phi(R_4^{-1}\vec{k}) \right) \right\} + \sum_{i=1}^{n_{\text{occ}}} \int_{L_2} \frac{d\vec{k}}{2\pi i} \cdot \frac{\partial}{\partial \vec{k}} \ln e^{i\theta_i(R_4^{-1}\vec{k})} \\
&= \text{Tr} \int_{L_1} \frac{d\vec{k}}{2\pi} \cdot \left\{ -i \left(\Psi^\dagger(\vec{k}) \frac{\partial}{\partial \vec{k}} \Phi(\vec{k}) \right) \right\} + n_2
\end{aligned} \tag{S.7}$$

where n_2 is an integer. Here, we have used the relation $\text{Tr}(ABC) = \text{Tr}(CAB)$. Additionally, we have used

$$\text{Tr} \left((\Psi')^\dagger(R_4^{-1}\vec{k}) \frac{\partial}{\partial \vec{k}} \Phi'(R_4^{-1}\vec{k}) \right) = \text{Tr} \left(\Psi^\dagger(R_4^{-1}\vec{k}) \frac{\partial}{\partial \vec{k}} \Phi(R_4^{-1}\vec{k}) \right), \tag{S.8}$$

since $\Phi'(\vec{k})$ ($\Psi'(\vec{k})$) is obtained by replacing the order of the column vectors in $\Phi(\vec{k})$ ($\Psi(\vec{k})$). This relation is originated from the assumption that the bands E_j and E_{j^*} are located at the left side of the real line gap in the complex plane of the energy distribution.

In the same approach, we obtain the equations,

$$\nu_3 = \text{Tr} \int_{L_1} \frac{d\vec{k}}{2\pi} \cdot \vec{A}(\vec{k}) + n_3, \tag{S.9}$$

$$\nu_4 = \text{Tr} \int_{L_1} \frac{d\vec{k}}{2\pi} \cdot \left\{ -i \left(\Psi^\dagger(\vec{k}) \frac{\partial}{\partial \vec{k}} \Phi(\vec{k}) \right) \right\} + n_4, \tag{S.10}$$

with integers n_3 and n_4 . By substituting Eqs. (S.7), (S.9), and (S.10) into Eq. (S.5), we obtain

$$\begin{aligned}
\nu_{\text{all}} &= 2\text{Tr} \int_{L_1} \frac{d\vec{k}}{2\pi} \cdot \vec{A}(\vec{k}) + 2\text{Tr} \int_{L_1} \frac{d\vec{k}}{2\pi} \cdot \left\{ -i \left(\Psi^\dagger(\vec{k}) \frac{\partial}{\partial \vec{k}} \Phi(\vec{k}) \right) \right\} + \sum_{i=2}^4 n_i \\
&= 2\text{Tr} \int_{L_1} \frac{d\vec{k}}{2\pi} \cdot \vec{A}(\vec{k}) + 2\text{Tr} \int_{L_1} \frac{d\vec{k}}{2\pi} \cdot \left\{ -i \left(\frac{\partial}{\partial \vec{k}} \Phi^T(\vec{k}) \right) \Psi^*(\vec{k}) \right\} + \sum_{i=2}^4 n_i \\
&= 2\text{Tr} \int_{L_1} \frac{d\vec{k}}{2\pi} \cdot \vec{A}(\vec{k}) - 2i \left(\sum_{j=1}^{n_{\text{occ}}} 1 \right) - 2\text{Tr} \int_{L_1} \frac{d\vec{k}}{2\pi} \cdot \left\{ -i \left(\Phi^T(\vec{k}) \frac{\partial}{\partial \vec{k}} \Psi^*(\vec{k}) \right) \right\} + \sum_{i=2}^4 n_i \quad (\text{S.11}) \\
&= 2\text{Tr} \int_{L_1} \frac{d\vec{k}}{2\pi} \cdot \vec{A}(\vec{k}) + 2\text{Tr} \int_{L_1} \frac{d\vec{k}}{2\pi} \cdot \vec{A}^*(\vec{k}) - 2in_{\text{occ}} + \sum_{i=2}^4 n_i \\
&= 4\text{Re} \left(\text{Tr} \int_{L_1} \frac{d\vec{k}}{2\pi} \cdot \vec{A}(\vec{k}) \right) - 2in_{\text{occ}} + \sum_{i=2}^4 n_i.
\end{aligned}$$

Here, we have used the integration by parts and the relation $\text{Tr}A = \text{Tr}A^T$. Therefore, from Eq. (S.11) and $\nu_{\text{all}} = n$ ($n \in \mathbb{Z}$), we obtain the quantization of the Berry phase in Eq. (19).

III. SIMPLIFICATION OF THE \mathbb{Z}_4 BERRY PHASE

We show the \mathbb{Z}_4 Berry phase can be computed from the data at the high-symmetry point Γ and M from the evaluation in Eq. (19),

$$\begin{aligned}
\nu &= \text{Tr} \int_{M' \rightarrow \Gamma} \frac{d\vec{k}}{2\pi} \cdot \vec{A}(\vec{k}) + \text{Tr} \int_{\Gamma \rightarrow M} \frac{d\vec{k}}{2\pi} \cdot \vec{A}(\vec{k}) \\
&= \text{Tr} \int_{M' \rightarrow \Gamma} \frac{d\vec{k}}{2\pi} \cdot \vec{A}(\vec{k}) + \text{Tr} \int_{\Gamma \rightarrow M} \frac{d\vec{k}}{2\pi} \cdot \left\{ -i \left(\Psi^\dagger(R_4^{-1}\vec{k}) \frac{\partial}{\partial \vec{k}} \Phi(R_4^{-1}\vec{k}) \right) \right\} + i \sum_{i=1}^{n_{\text{occ}}} \int_{\Gamma \rightarrow M} \frac{d\vec{k}}{2\pi} \cdot \frac{\partial}{\partial \vec{k}} \theta_i(R_4^{-1}\vec{k}) \\
&= \text{Tr} \int_{M' \rightarrow \Gamma} \frac{d\vec{k}}{2\pi} \cdot \vec{A}(\vec{k}) + \text{Tr} \int_{\Gamma \rightarrow M'} \frac{d\vec{k}}{2\pi} \cdot \left\{ -i \left(\Psi^\dagger(\vec{k}) \frac{\partial}{\partial \vec{k}} \Phi(\vec{k}) \right) \right\} + i \sum_{i=1}^{n_{\text{occ}}} \int_{\Gamma \rightarrow M'} \frac{d\vec{k}}{2\pi} \cdot \frac{\partial}{\partial \vec{k}} \theta_i(\vec{k}) \quad (\text{S.12}) \\
&= \text{Tr} \int_{M' \rightarrow \Gamma} \frac{d\vec{k}}{2\pi i} \cdot \vec{A}(\vec{k}) + in_{\text{occ}} - \text{Tr} \int_{M' \rightarrow \Gamma} \frac{d\vec{k}}{2\pi i} \cdot \vec{A}^*(\vec{k}) + \frac{1}{2\pi} \sum_{i=1}^{n_{\text{occ}}} (\theta(M') - \theta(\Gamma)) + in' \\
&= 2i \text{Im} \left(\text{Tr} \int_{M' \rightarrow \Gamma} \frac{d\vec{k}}{2\pi i} \cdot \vec{A}(\vec{k}) \right) - in_{\text{occ}} + \frac{1}{2\pi} \sum_{i=1}^{n_{\text{occ}}} (\theta(M') - \theta(\Gamma)) + n',
\end{aligned}$$

where n' denotes the integer. Since the high-symmetry point M' is identical to M , we obtain Eq. (21).

IV. TRIVIAL LOOPS OF THE EDGE SPECTRA

We show the case where the trivial loops of the energy spectra emerge. We plot the energy spectra under the periodic (open) boundary condition along x (y) direction for $(\delta t, \delta \gamma) = (-1, 1/2)$ and $(-1, -1/2)$, respectively [see Fig. 2]. In Fig. 2, there are trivial loops of the edge spectra between the bulk edge spectra. For these parameters, there are no hybrid higher-order topological skin modes.

V. \mathbb{Z}_2 INDICATOR WITH GENERALIZED MIRROR SYMMETRY

In the presence model, the Hamiltonian preserves the generalized mirror symmetry, namely, it satisfies

$$U_M H_{1D}(k) U_M^{-1} = H_{1D}^\dagger(-k), \quad (1)$$

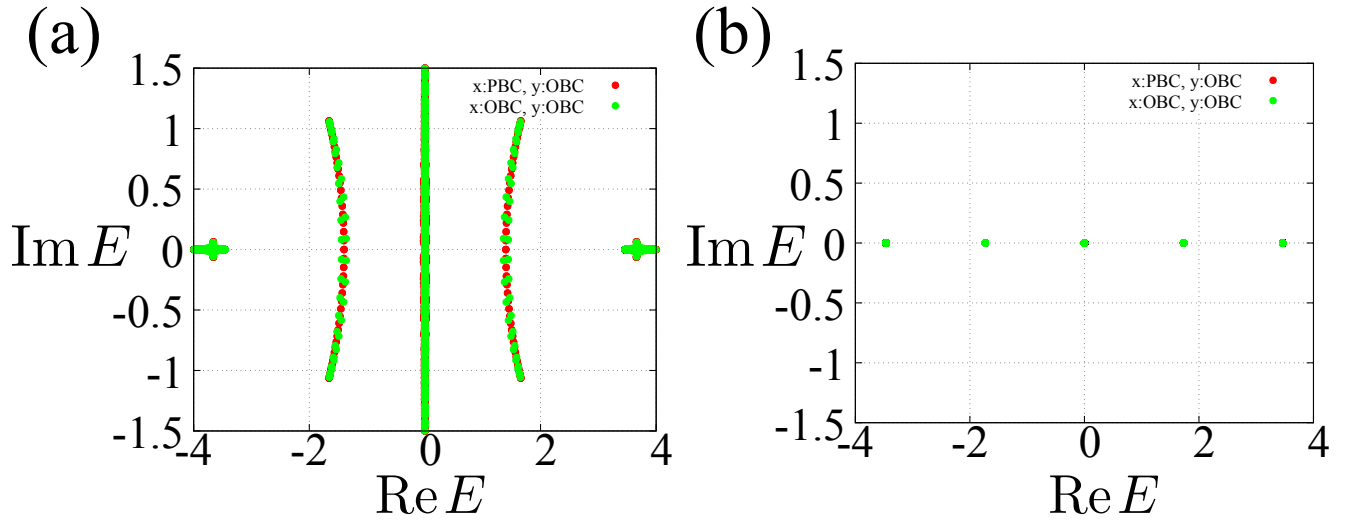


Fig. 2. (Color online) (a) and (b) show the energy spectrum for $(\delta t, \delta \gamma) = (-1, 1/2)$, and $(-1, -1/2)$, respectively. The red (green) dots show the energy spectrum under the periodic (open) boundary condition along the x direction.

where U_M denotes the unitary operator. The presence of this symmetry enables us to define \mathbb{Z}_2 indicator [3],

$$\mu := (-1)^w = \prod_{k=0, \pi} \det(H_{1D}(k) - E_{\text{ref}}). \quad (2)$$

Here, we have assumed that the reference energy E_{ref} is real. The nontrivial value of the indicator (i.e., $\mu = -1$) predicts the emergence of the skin effect, since it guarantees that w is nonzero. In the present system, the pair of \mathbb{Z}_4 Berry phase and this \mathbb{Z}_2 indicator predicts the emergence of the hybrid higher-order topological skin modes. However, μ cannot predict the position of the hybrid higher-order topological skin modes since we cannot see the difference between $w = 1$ and $w = -1$.

-
- [1] S. Tsubota, H. Yang, Y. Akagi, and H. Katsura, Phys. Rev. B **105** L201113 (2022).
 [2] K. Chen and A. B. Khanikaev, Phys. Rev. B **105**, L081112 (2022).
 [3] R. Okugawa, R. Takahashi, and K. Yokomizo, Phys. Rev. B **103**, 205205 (2021).